Fibers and Polymers 2022, Vol.23, No.9, 2526-2538
DOI 10.1007/s12221-022-0005-x

ISSN 1229-9197 (print version)
ISSN 1875-0052 (electronic version)

Synthesis and Characterization of the Temperature Controllable Shape Memory of Polycaprolactone/Poly(ethylene terephthalate) Copolyester

Fu-Ting Yang[1]*, Yu-Ming Chen[2], and Syang-Peng Rwei[1,3]*

[1]*Institute of Organic and Polymeric Materials, National Taipei University of Technology, Taipei 10608, Taiwan, ROC*
[2]*Taiwan Textile Research Institute, New Taipei 23674, Taiwan, ROC*
[3]*Research and Development Center of Smart Textile Technology, National Taipei University of Technology, Taipei 10608, Taiwan, ROC*

(Received January 3, 2022; Revised April 1, 2022; Accepted May 1, 2022)

Abstract: In this study, a series of novel controllable shape-memory polymers composed of poly(ethylene terephthalate) (PET) and poly(ε-caprolactone) (PCL) were synthesized using the one-pot method and were spun using the melt spinning process. The chemical structure and composition, thermal properties, crystallization properties, mechanical properties, and shape-memory behavior of these copolymers were characterized. The results revealed that the incorporation of a flexible PCL segment achieved random copolymers. The aliphatic PCL segment decreased the melting point, crystallinity, and glass transition temperature. The thermal stability of the synthesized PET-*co*-PCLs was higher than that of the blended polymers, and the decomposition temperature of PET-*co*-PCL-30 % reached 377.2 °C. The shape recovery ratio of PET-*co*-PCL-30 % was between 38.32 % and 82.69 % and was temperature dependent. The as-spun PET and PET-*co*-PCL fibers were melt spun at a winding rate of 1,000 m/min. The strength values of the fibers ranged from 2.16 to 1.2 gf/den depending on the increase in PCL content. Because of the biocompatibility of both PET and PCL and the shape-memory features of these copolyesters, PET-*co*-PCL fibers can be applied in intelligent textiles.

Keywords: Poly(ethylene terephthalate), Polycaprolactone, Copolyester, Melt spinning, Shape memory

Introduction

Poly(ethylene terephthalate) (PET) possesses remarkable thermal stability, tensile strength, and chemical resistance; is low cost; and has low energy requirements, making it ideal for use in a wide range of industrial applications, such as in textile fiber, film, bottles, and packaging [1-6]. The production capacity of PET exceeded 50 million tons in 2019 and is still increasing rapidly [7]. However, a large amount PET waste, known as white pollution, is produced, causing environmental problems [8,9], and harmful soot is generated because the main raw materials of PET are nonrenewable petrochemical resources that do not decompose easily under natural or composting conditions [10]. To solve these environmental problems, two recycling strategies can be adopted. The first is to replace nonrenewable resources as raw material with biomass monomers obtained from nature [11-13], and the second is the introduction of biodegradable segments into the main PET chain to improve the material's biodegradability [14].

Recently, the synthetic aliphatic polyester poly(ε-caprolactone) (PCL) has attracted considerable attention, notably for medical products, shape-memory applications, and packaging, because of its characteristics of biodegradability and biocompatibility, and it has been approved by the U.S. Food and Drug Administration for use in the human body [15-19].

Based on the aforementioned recycling strategies, two major techniques, namely mechanical blending and chemical reaction, are used to modify nonbiodegradable aromatic polyesters into ecofriendly biodegradable polymers [20,21]. The mechanical method, in which nonbiodegradable aromatic polyester is blended with biodegradable aliphatic polyester, is a relatively low-cost and straightforward solution. Several articles have reported that blending methods are simpler and easier to control than the chemical method. For example, Lim *et al*. studied the effect of the blending time [22] and molecular weight of PCL [23] on the block characteristics of PET/PCL blends, and Saaoui *et al*. [24] studied the compatibilization of PET/PCL blends using montmorillonites. Saeed and Park [25] investigated the thermal properties of PBT/PCL blends. It is also another way to enhance the biodegradability of aromatic polyester through copolymerization. Modification through copolymerization mainly focuses on the substitution of low-molecular-weight biodegradable diols [26-28], such as 1,3-propanediol, 1,4-butanediol, polyethylene glycol, and 2,2-dialkyl-1,3-propanediol and aliphatic diacids [29-31], and the addition of succinic acid, adipate acid, and sebacic to the aromatic backbone of the polymer main chain.

Although several recycling methods are available, only 20-30 % of PET is recycled worldwide [7]. Therefore, development of ecofriendly applications of PET are urgently required. However, the low thermal stability of aliphatic chains makes it challenging to obtain high-performance polymer alloys by blending different compositions of aromatic and aliphatic polyesters. Studies have described that the blending time of these semiaromatic polyester alloys should be minimally controlled to avoid the thermal

*Corresponding author: chris10281028@gmail.com
*Corresponding author: f10714@ntut.edu.tw

degradation of the aliphatic segment. However, reducing the blending time usually leads to immiscibility because of the lack of a transesterification reaction between the components [23]. Consequently, the blending of semiaromatic polyesters results in limited feasibility of the method, weak properties, and a low-grade product [32].

In this study, the temperature controllable shape-memory copolyesters of PET and PCL were copolymerized using the one-pot method with a CL content of 10-30 parts per hundreds of resin (phr) and were then spun using the melt spinning process. The shape-memory behavior, chemical structure and composition, thermal properties, crystallization properties, and mechanical properties were investigated. The as-spun PET and PET-*co*-PCL fibers were melt spun at a winding rate of 1,000 m/min. In addition, the tensile properties of the fibers were characterized. Because of the biocompatibility of both PET and PCL and the shape-memory property of these copolymers, the PET-*co*-PCL fibers can be applied in intelligent textiles.

Experimental

Materials

The following reagents were used in the experiment: terephthalate acid (TPA; Oriental Petrochemical, Taoyuan, Taiwan), ethylene glycol (EG, commercial-grade; Emperor Chemical, Taipei, Taiwan), titanium(IV) butoxide (TBT, 97 %; Aldrich, St Louis, MO, United States), trifluoroacetic acid-d (TFA-d, 99.5 %; Aldrich), phenol (97 %; Aencore Chemical, Surrey Hills, Australia), 1,1,2,2-tetrechloroethane (97 %; Showa Chemical Industry, Tokyo, Japan), and acetone (Sigma Aldrich, Burlington, VT, United States). All the reagents were used as received without further purification. The recycled PCL (M_w=50,000 g/mole) was provided by TSM Smart Materials (Taoyuan, Taiwan).

Synthesis of PET and PET-*co*-PCL Copolymers

The synthesis process is presented in Scheme 1. For the synthesis of the PET prepolymer and PET-*co*-PCL copolymers, a one-pot polycondensation method was adopted. A stainless-steel 2-L reactor equipped with a mechanical stirrer, nitrogen inlet and outlet, temperature sensor, distillation column, and vacuum system was used. In brief, first, the TPA, EG, and TBT catalysts were charged in the reactor. An esterification reaction between TPA and EG was performed by stirring at 50 rpm at 250 °C under a nitrogen flow at a pressure of 3 bar. The diester to diol molar ratio was set at 1:1.2, and the amount of TBT was retained at 400 ppm based on the theoretical amount of oligo(ethylene terephthalate). The degree of esterification was determined

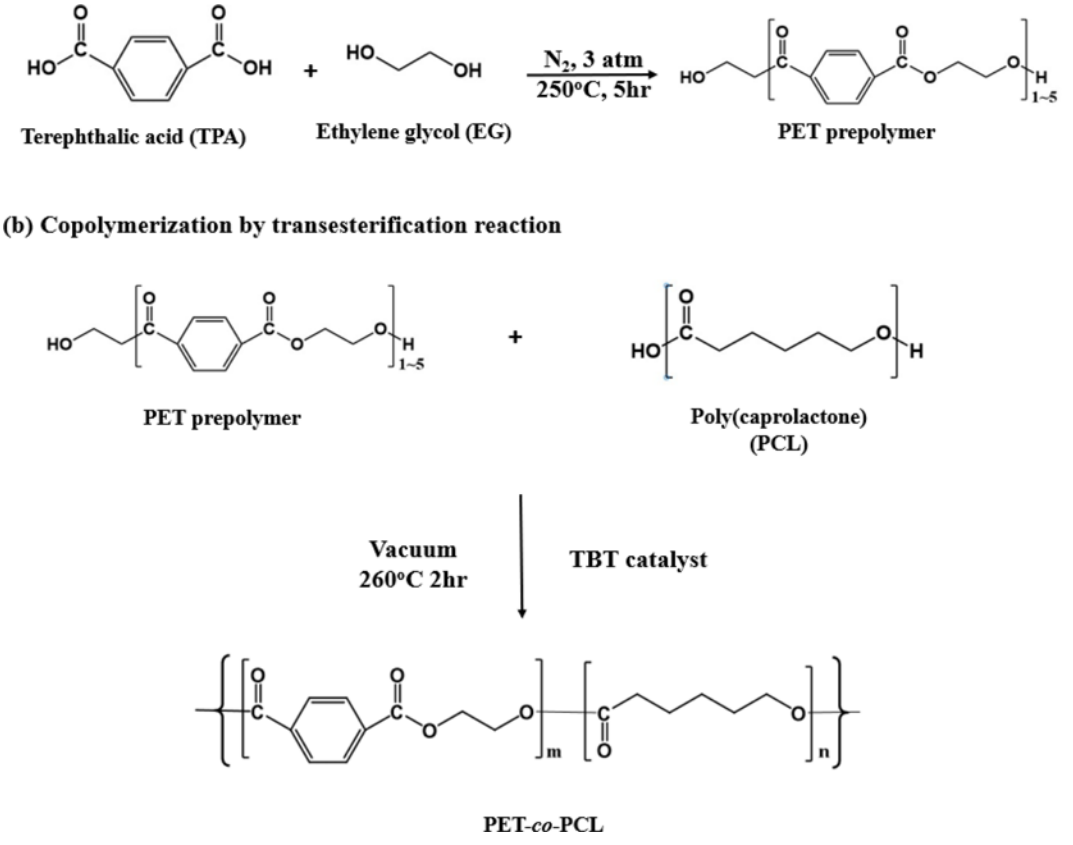

Scheme 1. (a) Synthesis of the PET prepolymer and (b) copolymerization using a transesterification reaction.

by measuring the amount of cool-condensed H_2O, and the endpoint of the esterification reaction was selected as the esterification degree of more than 90 %. For the polycondensation reaction, the PCL was added to the reactor under a nitrogen atmosphere at 200 °C. After the reactants were moderately mixed to form a homogenous melt, the polycondensation reaction was conducted by gradually increasing the temperature from 200 to 260 °C and decreasing the pressure from 760 to less than 1 Torr over a 30-min period and then maintaining the temperature and vacuum to remove excess diols and by-products until the end of the reaction. The reaction lasted approximately 2-3 h. The exact endpoint of the polycondensation reaction was selected as the stirring torque of 1.2-1.5 times the reference value. Finally, the melted polymer was plunged into ice water, pelletized using a granulator into approximately 2-mm pellets, dried in a vacuum oven at 105 °C for 4 h, and stored in an aluminum foil sealed bag with a desiccant to keep the pellets dry until further analysis and processing. A series of PET-*co*-PCL copolyesters with the transesterification product to PCL feed weight ratios of 100:10, 100:20, and 100:30 were produced and designated as PET-*co*-PCL-10 %, PET-*co*-PCL-20 %, and PET-*co*-PCL-30 %, respectively.

Nuclear Magnetic Resonance Spectroscopic Analysis

A Bruker Avance III HD-600 MHz nuclear magnetic resonance (NMR) spectrometer (Bruker, Germany) was used to identify the synthesized copolymers. In brief, 5-10 mg of polymers was fully dissolved through ultrasonic shock in 1 m*l* of TFA-d in a 10-m*l* vial and then transferred to 5-mm NMR spectroscopic analysis (^{1}H-NMR) sample tubes. All the experiments were performed at 25 °C, with 64 recorded scans.

Fourier Transform Infrared Spectroscopy

For Fourier transform infrared spectroscopy (FT-IR), the samples were prepared as thin films of approximately 300 μm by using hot-pressure mechanics at a temperature of approximately 20-30 °C above the melting temperature. The FT-IR spectra from 4,000 to 650 cm^{-1} were recorded using a PerkinElmer Spectrum One spectrometer (Waltham, MA, United States) in the attenuated total reflection mode at a resolution of 4 cm^{-1}, with 16 scans.

Intrinsic Viscosity

The intrinsic viscosity [η] of the polymers was measured using the ASTM D4603 method. The polymers were dissolved in a mixture of phenol and 1,1,2,2-tetrachloroethane at a 60:40 weight ratio at a concentration of 0.5 g dl^{-1}. The intrinsic viscosity measurement was performed on a Cannon Ubbelohde Type 1B Viscometer at 30±0.05 °C. The [η] values of the copolyesters were calculated using the Billmeyer relationship [33]:

$$[\eta] = 0.25[\eta_r - 1 + 3\ln(\eta_r)] \quad (1)$$

where η_r is the relative viscosity.

Differential Scanning Calorimetry

Differential scanning calorimetry (DSC) measurements were performed using a PerkinElmer DSC 8000 system. Samples were cut from the pellets and dried in a vacuum oven at 105 °C for 1 h. Each sample had a mass of 4-6 mg and was sealed in an aluminum pan. The measurements were conducted over a temperature range of 0 to 280 °C at a heating rate of 10 °C/min and a nitrogen flow rate of 20 m*l*/min. The conventional triple-cycle heating-cooling-heating process was employed. The temperature was maintained at 280 °C for 3 min in the first heating stage to remove the thermal history. The melting temperature (T_m), crystallization temperature (T_c), melting enthalpy (ΔH_m), and crystallization enthalpy (ΔH_c) were determined as the maximum of endothermic peaks, the minimum of exothermic peaks, and the corresponding integral values of the peaks in the first cooling cycle and the second heating cycle, respectively. To study the influence of the process conditions on crystallization properties, DSC measurements were performed on the fibers. To perform these measurements, the samples were used without further drying. The first heating curve was obtained over the temperature range from 0 °C to 280 °C at a heating rate of 10 °C/min and a nitrogen flow rate of 20 m*l*/min.

Dynamic Mechanical Analysis

For dynamic mechanical analysis (DMA), approximately 1-mm-thick specimens were obtained using a hot-press at a temperature of 20-30 °C, which was above the melting temperature, and were then cut into narrow strips of 20×5 mm^2. DMA (TechMax DMS 6100) was used to measure the viscoelastic properties of the specimens. The samples were analyzed in the tension mode with a minimum force of 100 mN over the temperature range of -100 to 250 °C at a rate of 5 °C/min and a fixed frequency of 1 Hz.

Thermogravimetric Analysis

Thermogravimetric (TGA) analyses were performed on a HITACHI TGA STA 7200 apparatus. The samples, weighing approximately 5-6 mg, were placed in a ceramic furnace, and the test was conducted under a nitrogen atmosphere at a flux rate of 100 m*l*/min, with heating from 30 to 600 °C at a rate of 10 °C/min. The characteristic onset of the degradation temperature was determined from the TGA curve at 5 % weight loss ($T_{d\text{-}5\,\%}$). For the isothermal TGA test, the samples were heated to 270 °C at a rate of 10 °C/min, and that temperature was then maintained for 3 h.

Wide-angle X-ray Diffraction

For wide-angle X-ray diffraction analysis, approximately

1-mm-thick specimens were obtained using a hot-press at a temperature of 20-30 ℃, which was above the melting temperature, and were then cut into squares of 10×10 mm^2. The X-ray diffraction patterns of the film samples were recorded using the Panalytical X Pert^3 Powder instrument equipped with a CuKα radiation source (λ=0.154 nm) and were then verified in the 2θ range of 10-40 ° with a scanning speed of 0.2 °/min.

Tensile Test

For tensile tests, dumbbell-shaped specimens were prepared through injection molding (Minijet pro; Thermo Scientific). The polymer was fed into a feeder and preheated for 5 min. After the polymer had completely melted, it was injected into the dumbbell-shaped mold at an injection pressure of 350 bar, and a pressure of 250 bar was maintained for 30 s to remove any bubbles. The injection temperature was 30 ℃ higher than the melting point, and the mold temperature was half that of the injection temperature. Tensile properties were investigated using a Cometech QC-508M2F tensile testing machine, and the dumbbell size and conditioning were in line with ASTM D638 type IV standards. Each sample was analyzed at a crosshead speed of 100 mm/min. Young's modulus, elongation at break, and tensile strength were evaluated using the stress-strain data. The average values were obtained from five specimens.

Shape-memory Properties

The dumbbell-shaped specimens used for the tensile test were also employed to evaluate shape-memory properties. The specimens were maintained at 60±2 ℃ and stretched at a rate of 50 mm/min using a Cometech QC-508M2F tensile testing machine until they reached the required strain (ε_m); they were then cooled to room temperature while maintaining ε_m. The specimens were then removed from the machine and left for 5 min to ensure stress release, and fixed strain (ε_f) was then measured. The fixed specimen was then reheated to a given temperature between 40 and 100 ℃ to induce the recovery process, and the final recovered strain (ε_r) was recorded. The shape fixation ratio (R_f) and shape recovery ratio (R_r) were calculated as follows [34]:

$$R_f = \frac{\varepsilon_f}{\varepsilon_m} \times 100\% \quad (2)$$

$$R_r = \frac{(\varepsilon_f - \varepsilon_r)}{\varepsilon_f} \times 100\% \quad (3)$$

The shape-memory properties of the fibers were measured using the aforementioned procedure. The length of fiber used was 10 mm, and DMA was used to control the temperature and elongation.

Fiber Spinning

The fibers were fabricated using a melt spinning technique. Before spinning, the synthesized polymer chips were dried at 105 ℃ in a vacuum oven for 3-5 h. Spinning was then performed using a single-end spinning machine with a self-developed winder. The twin-screw extruder (Thermo Scientific Process 11 Parallel Twin Screw Extruder) had a diameter of 11 mm, and an L/D ratio of 40 was used. The spinneret had a diameter of 1.5 mm and a single hole. The winding speed was fixed at 1,000 m/min, and the specification of the filaments was approximately 10-15 d/f.

Mechanical Properties of the Fibers

The tenacity and elongation of the fibers were determined using a automatic tensile tester (Textechno, FPAC, No. 35032) with a gauge length of 250 mm, and a reasonable rate of extension was selected to ensure that the breaking time of the tested fibers was maintained at 20±5 s.

Results and Discussion

Synthesis and Structure Characterization of the Copolyesters

TPA, EG, and PCL were utilized for the synthesis of PET-*co*-PCLs following the one-pot method, as illustrated in Scheme 1. PET-*co*-PCLs with a PCL content between 10

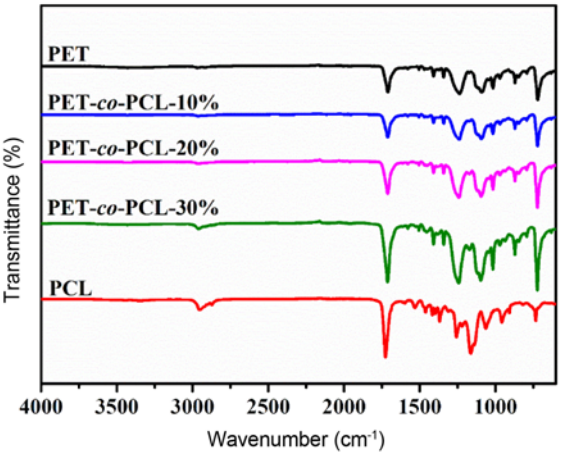

Figure 1. Infrared spectra of the PET, PCL, and PET-*co*-PCLs.

Table 1. Assignment of the vibration signals through FT-IR of the synthesized polymers

Wavenumber (cm^{-1})	Type of vibration
2963	Asymmetric stretch, CH_2
2967	Symmetrical stretching, CH_2
1713	Carbonyl stretch, C=O
1239	Asymmetric stretch, C-O-C
1167	Stretching of the amorphous phase of C-C and C-O
871	Phenyl, CH

and 30 phr were prepared. TBT was chosen as the catalyst for condensation polymerization. For comparison, PET was synthesized using the same procedure.

The chemical structure of PET, PCL, and PET-*co*-PCLs was determined using FT-IR (Figure 1 and Table 1) and ^{1}H-NMR (Figure 2), and the presence of PET and PCL segments in the PET-*co*-PCLs was verified. In the spectra, the absorption bands at 1,726 and 1,713 cm^{-1} were attributed to the C=O stretching vibrations of the CL units and PET species of PET-*co*-PCLs, respectively. The structure of the CL units was also verified by the vibration signal at 1,164 cm^{-1}, which is associated with the amorphous zones of the PCL [35]. The transmittance of the peak at 1,755 and 1,164 cm^{-1} became stronger with the increasing CL content. Thus, signals associated with the PET and PCL units were present in the PET-*co*-PCL spectra, indicating that the PET-*co*-PCLs had been synthesized successfully through the one-pot method.

To further investigate the chemical structure of the PET-*co*-PCLs and verify that copolymerization had occurred, ^{1}H-NMR analysis of the PET-*co*-PCL spectra was conducted. The signal assignments for the possible segment units of the PET-*co*-PCLs are listed in Figure 2. These spectra were compared with those of neat PET and recycled PCL, revealing several new resonances. Characteristic peaks associated with the PET-*co*-PCLs were observed at δ=4.5-

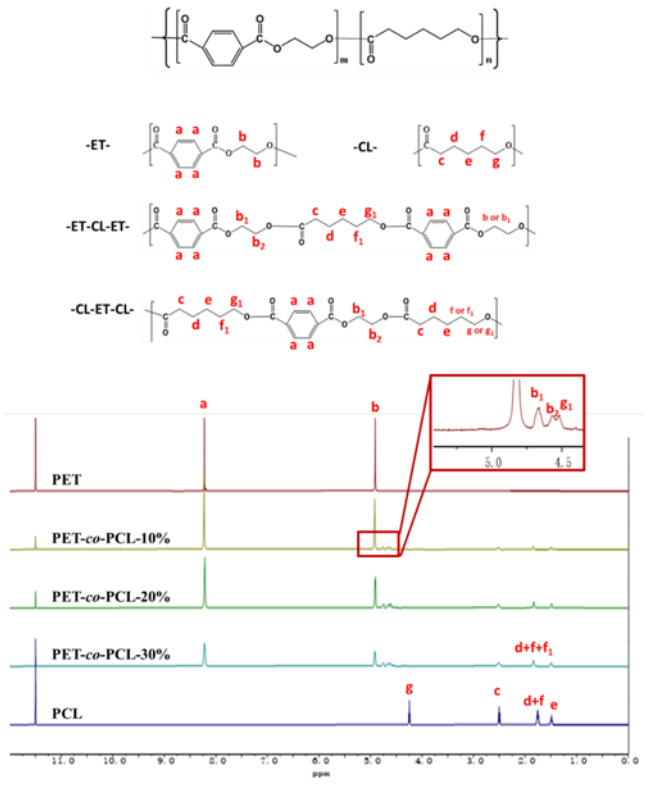

Figure 2. ^{1}H-NMR analysis of the PET-*co*-PCLs and the signal assignment of possible molecular segment arrangements.

Table 2. Composition obtained through ^{1}H-NMR of the PET, PCL, and PET-*co*-PCLs

Sample	A_{TA}	A_{EG}	m	n	Area%	R
PET	1	1	-	0	0	-
PET-*co*-PCL-10 %	1	0.83	5.88	0.99	9.6	1.18
PET-*co*-PCL-20 %	1	0.69	3.23	1.09	17.8	1.23
PET-*co*-PCL-30 %	1	0.61	2.56	1.30	25.3	1.16
PCL	0	0	0	-	0	-

4.7 ppm (b_1, b_2, and g_1) and δ=1.8 ppm (f_1), indicating a slight downfield shift. In addition, the characteristic PET unit peaks appeared at δ=8.22-8.34 (a) and δ=4.8 (b). The characteristic peaks of the PCL units presented at δ=4.25 (g) in the ^{1}H-NMR spectra.

The PET-*co*-PCL ^{1}H-NMR and FT-IR spectra verified that PET and PCL copolymerization had successfully occurred. The values of the average repeating units of the CL and ET segments, *n* and *m*, in each macromolecule were obtained from the change in the peak area assigned to the EG unit between two TA units, X_{EG}, which was calculated using equation (4) [22]:

$$X_{EG} = \frac{A_{TA} - A_{EG}}{A_{TA}} \tag{4}$$

where A_{EG} and A_{TA} are the peak areas assigned to the EG (δ=4.8) and TA units (δ=8.22-8.34), respectively; the environmental difference in the copolymer EG unit compared with that of the PET homopolymer indicates a loss in A_{EG}, resulting in a X_{EG} value of greater than 0. The increase in X_{EG} indicates a decrease in the ET sequence length, denoted as *m*, in the copolyester chain. Therefore, *m* can be calculated as follows:

$$m = \frac{1}{X_{EG}} \tag{5}$$

However, X_{CL}, the molar fraction of the CL units in the copolyesters, is expressed by equation (6), and *n* can then be obtained from equation (7):

$$X_{CL} = \frac{n}{n+m} \tag{6}$$

$$n = \frac{m \times X_{CL}}{1 - X_{CL}} \tag{7}$$

The results of equations (4)-(7) (Table 2) reveal a relationship between the number of average repeating units and the CL content. The number of average repeating units of the ET blocks decreased with an increase in the CL content. The area ratios of the peaks corresponding to the species representing the bonding of CL with ET (b_1, b_2, and g_1) to the total peak area are also listed in Table 2. At a higher CL content, the ratios of the areas tended to improve,

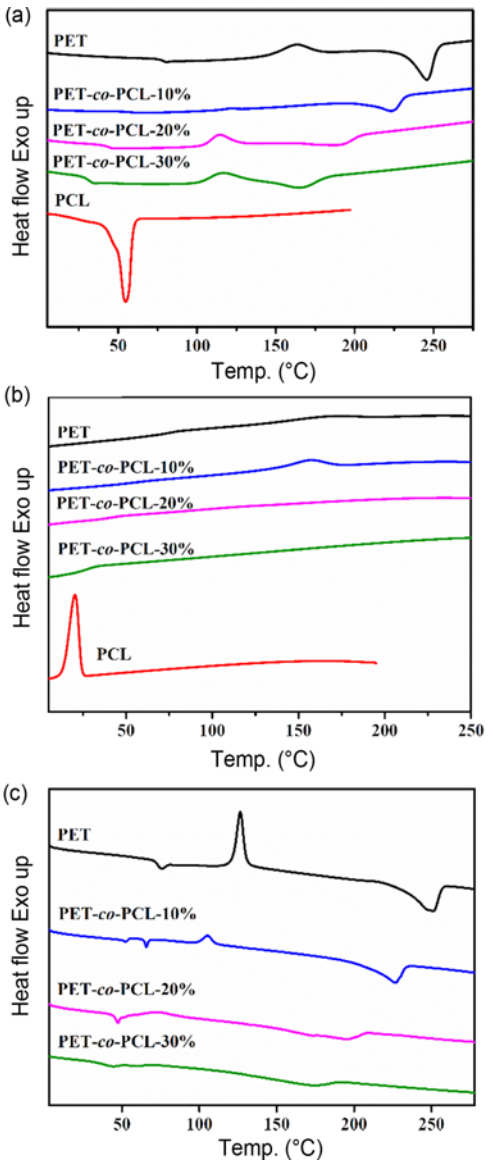

Figure 3. DSC thermograms of the PET, PCL, and PET-*co*-PCLs; (a) second heating scan of pellets, (b) cooling scan of pellets, and (c) first heating scan of fibers.

verifying PET and PCL copolymerization.

The degree of randomness R was determined by the number fractions of these two ^{1}H-NMR segments (Figure 2 and Table 2) through equation (8) [36]:

$$R = \frac{1}{n} + \frac{1}{m} \tag{8}$$

where n and m represent the number-average sequence length of CL and ET, respectively. The randomness of each PET-*co*-PCL species is close to 1, indicating a random distribution for each species.

Thermal, Mechanical, and Crystallization Properties of the Copolyesters

PET possesses superior thermal properties because of its aromatic chemical structure and appropriate molecular weight and polydisperse index. As mentioned, the copolyesters prepared in this study were random copolymers. The content of the CL chain segment may have caused a change in the crystal structure of the copolyesters. The DSC curve in Figure 3 reveals that the heat flow is dependent on the composition and process conditions of the PET-*co*-PCLs. Their calorimetric parameters and T_g measured through DMA are provided in Table 3. As shown in Figure 4, the T_g values of the PET-*co*-PCLs decreased with an increase in the CL content from 90.1 °C (PET) to 30.3 °C (PET-*co*-PCL-30 %). The melting temperature of the PET-*co*-PCLs decreased with the increasing CL content. As the CL content increased to more than 10 phr, the crystallization peak of PET-*co*-PCL-20 % and PET-*co*-PCL-30 % disappeared. Incorporation of the short aliphatic CL segment may have improved the motility of the molecular chain and decreased the chain's regularity. As CL chain segments were introduced, the degree of crystallinity (X_c) in PET-*co*-PCL-20 % and PET-co-PCL-30 % was reduced to almost zero at the given cooling rate, which may be because the short CL chain segment decreased the regularity of the chain, resulting in a decrease in the crystallization rate. With regard to PET-*co*-PCL-10 %, the value of X_c increased as the molecular chain's motility was enhanced. These two effects had the

Table 3. Thermal properties and intrinsic viscosity of the PET, PCL, and PET-*co*-PCLs

Sample	1st heating scan of fiber				1st cooling scan of pellet		2nd heating scan of pellet				DMA scan of pellet	Intrinsic viscosity	Crystallinity
	T_g (°C)	T_{cc} (°C)	T_m (°C)	ΔH_m (J/g)	T_c (°C)	ΔH_c (J/g)	T_g (°C)	T_{cc} (°C)	T_m (°C)	ΔH_m (J/g)	T_g (°C)	[η] (dL/g)	X_c (%)
PET	72.9	126.5	251.4	39.5	173.4	-20.0	74.9	162.6	245.6	37.5	90.1	0.57	16.7[a]
PET-*co*-PCL-10 %	65.7	105.2	227.3	40.6	157.6	-29.3	60.2	121.3	223.6	28.4	64.3	0.56	24.4[a]
PET-*co*-PCL-20 %	45.0	71.3	197.8	37.3	N/A	N/A	43.1	114.6	190.4	22.6	44.2	0.59	N/A[a]
PET-*co*-PCL-30 %	32.6	69.7	173.6	21.7	N/A	N/A	31.5	115.03	164.3	8.19	30.3	0.56	N/A[a]
PCL	-	-	-	-	20.6	-44.8	N/A	N/A	54.3	42.5	-38.4	1.07	32.1[b]

[a]Crystallinity of PET and PET-based copolymers is calculated by dividing ΔH_c by 119.8 J/g, which is the enthalpy of 100 % crystalline PET and [b]crystallinity of PCL is calculated by dividing ΔH_c by 139.5 J/g, which is the enthalpy of 100 % crystalline PCL.

opposite effect on the crystallinity of PET. However, a recrystallization peak for all the copolymers was observed in the second DSC heating curves (Figure 3(a)), which means that their crystallinity could be enhanced through annealing under appropriate conditions. Table 3 summarizes the changing trend in T_g, T_m, and T_c, revealing that as the CL content increased, the influence of T_g became weaker, whereas T_m and T_c decreased substantially. Compared with the pellet samples, the fiber samples exhibited a marginal shift in T_g and T_m to a higher temperature and increased melting enthalpy, respectively. This may result from the high internal tensile stress produced under the melt spinning conditions. The lower cold crystallization temperature (T_{cc}) of the fiber sample suggested that during the melt spinning process, thermal molecular orientation increased in the fibers, enabling cold crystallization to occur at a lower temperature.

Figure 5 depicts the XRD patterns of PET, PCL, and the PET-*co*-PCLs. To increase their crystallinity, all the copolymers were annealed in a vacuum oven at 90 °C, except for PCL, which was annealed at 40 °C for 1 h. All the PET-*co*-PCLs exhibited seven feature peaks at 2θ=15.8 °, 17.2 °, 21.5 °, 22.5 °, 25.8 °, 27.5 °, and 32.5 °, which could be ascribed to PET crystals. There were no crystal peak of PCL, indicating that the copolyesters contained only PET crystals. This result is consistent with the DSC results, suggesting that the CL segment was excluded from the crystal during the crystallization process, and that the CL segment alone did not contribute to crystal formation. The peak areas of PET-*co*-PCL-20 % and PET-*co*-PCL-30 % were similar, indicating that the PET and PCL copolymers achieved almost the same X_c values under suitable annealing conditions.

The thermal stability of a polymer is a key property that affects its application field; a poor thermal decomposition temperature (T_d) can restrict its applications. Aliphatic polyesters, such as poly(lactic acid) and poly(ether-ester), have lower thermal stability than aromatic polyesters, with a

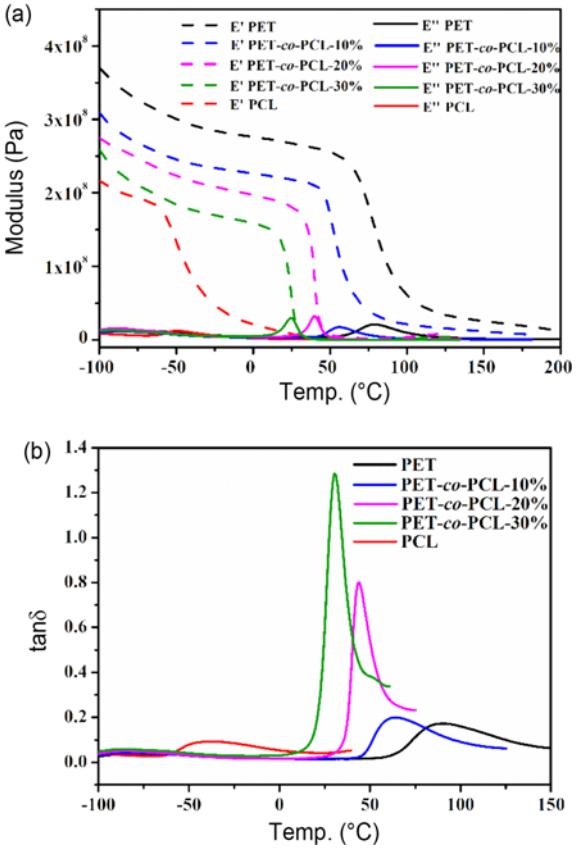

Figure 4. DMA curves of the PET, PCL, and PET-*co*-PCLs; (a) storage and loss modulus and (b) tan *δ*.

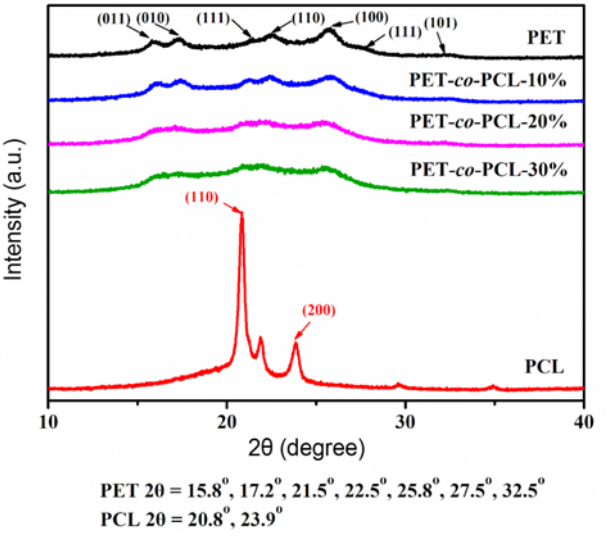

Figure 5. X-ray patterns of the PET, PCL, and PET-*co*-PCLs.

Table 4. Thermal stability of the PET, PCL, and PET-*co*-PCLs

Sample	$T_{d\text{-}5\,\%}$ (°C)	$T_{d\text{-}max}$ (°C)	T_d(3h) (%)	T_d(3h, ava.) (%)	Char yield at 600 °C (%)
PET	397.9	440.5	99.2	99.2	15.4
PET-*co*-PCL-10 %	386.8	432.5	98.7	98.1	12.6
PET-*co*-PCL-20 %	381.1	431.9	97.7	97.1	12.0
PET-*co*-PCL-30 %	377.2	422.7	97.1	96.3	11.4
PCL	330.5	398.0	86.6	86.6	2.6

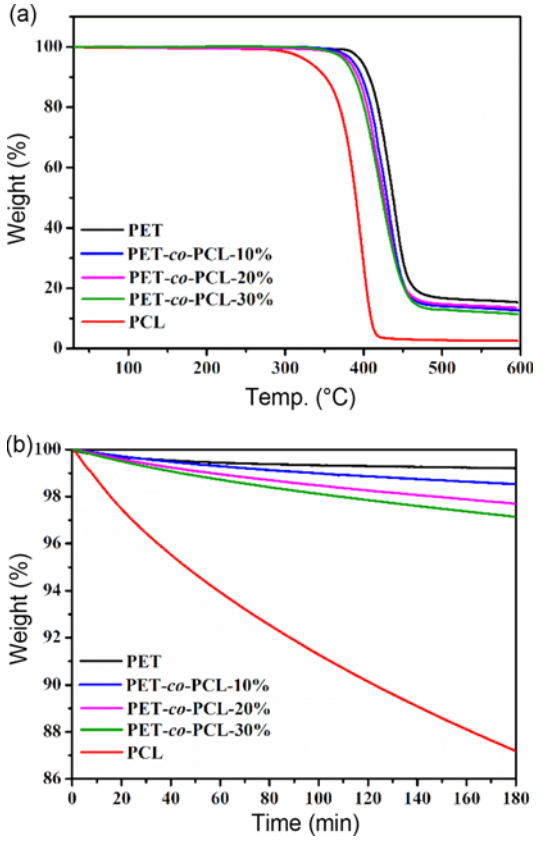

Figure 6. TGA curves of the PET, PCL, and PET-*co*-PCLs; (a) normal TGA test from 30 °C to 600 °C and (b) isothermal TGA test at 270 °C for 3 h.

few exceptions. The TGA thermograms in Figure 6 demonstrate that incorporating a short CL segment decreased the initial degradation temperature compared with that of a PET homopolymer. Table 4, which summarizes the results of Figure 6, reveals that the $T_{d\text{-}5\,\%}$ values of the copolymers of PET-*co*-PCL-10 %-PET-*co*-PCL-30 % were in the range of 386.8-377.2 °C, which was lower than that (397.9 °C) of a PET homopolymer. The increasing PCL content from 0 to 30 phr indicates the dilution of the stable benzene ring and a decrease in the degradation temperature. To understand the long-term thermal stability of the copolymers, an isothermal TGA test was conducted. The samples were tested at 270 °C for 3 h; the 3-h thermal stability results, T_d(3h), and the theoretical values calculated based on the number-average value of T_d(3h) for PET and PCL [T_d(3h, ava.)] are presented in Table 4. Although $T_{d\text{-}5\,\%}$ decreased 22.7 °C for PET-*co*-PCL-30 % compared with neat PET, the copolymers exhibited an excellent T_d(3h) of 97.1 %, indicating that a weight loss of only 2.9 % occurred at 270 °C for 3 h. T_d(3h) was higher than T_d(3h, ava.), suggesting that the thermal stability of the synthesized PET-*co*-PCLs was higher than that obtained for the simple mixing of PET and PCL. However, the temperatures required in all the subsequent

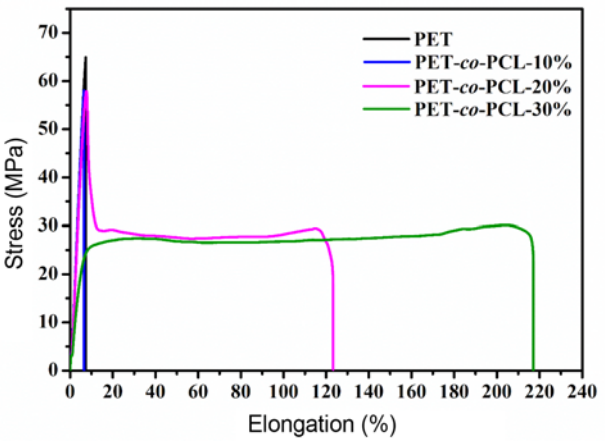

Figure 7. Tensile strength curves for PET and the PET-*co*-PCLs.

processes related to melt spinning to produce fabric or textured yarn were much lower than 270 °C.

DMA was used to determine the T_g of polymers. The T_g values were defined as the peak of the tan δ curve (Figure 4(b)). The PET homopolymer sample had the highest T_g value because it possessed the highest ratio of benzene rings, which suppressed chain mobility. All the obtained T_g values are tabulated in Table 3. These values suggest that T_g decreased with the increasing CL content because of the flexibility of the aliphatic segments, which constitute a substantial amount of the free volume and can easily rotate in the absence of a benzene structure. The resulting copolymer T_g decreased from 64.3 °C for PET-*co*-PCL-10 % to 30.3 °C for PET-*co*-PCL-30 %. Notably, PET-*co*-PCL-30 % had a T_g of 30.3 °C, which is close to body temperature, indicating its potential for use in phase change materials for clothes.

The mechanical properties of the polymer dumbbell-shaped specimens are presented in Table 5 and Figure 7. The tensile strength decreased and elongation increased as the CL content gradually increased. The copolymers exhibited an optimized integral mechanical property, a substantial

Table 5. Mechanical properties of the PET, PCL, and PET-*co*-PCLs for the dumbbell-shaped specimens

Sample	Tensile strength (MPa)	Elongation at break (%)	Young's modulus (MPa)
PET	64.9±2.7	7.4±0.3	1037±11.1
PET-*co*-PCL-10 %	58.0±2.3	6.5±0.2	999±13.4
PET-*co*-PCL-20 %	57.9±2.2	123.3±8.5	947±12.9
PET-*co*-PCL-30 %	30.2±2.0	217.1±15.8	545±10.4
PCL	23.2±1.8*	>1200[a]	95±8.8

[a]The elongation at break of PCL was greater than the maximum of the tensile testing machine.

elongation increment from 6.5 % to 123 %, and a small decrease in the maximum tensile strength and Young's modulus from 58.0 to 57.9 MPa and 999 to 947 MPa, respectively, when the CL content was 20 phr.

Shape-memory Properties of the Copolyesters

In general, a shape-memory polymer (SMP) is composed of two phases, stationary and reversible phases. Initially, a polymer product possesses a permanent shape. After being subjected to specific external stimuli, such as heat, light, magnetism, electricity, pH, and moisture [37-42], the interaction force of the reversible phase decreases, and that of the stationary phase remains unchanged. At this point, an external force can be applied to deform the reversible phase into the desired shape [43]. After the external stimulus has been removed, the physical or chemical crosslinking of the reversible phase is restored, and the polymer shape can be temporarily fixed without applying an external force. In the SMP field, this stimulus-deformation-fixation process is called programming. With regard to the SMP recovery process, the external stimulus can be reapplied to induce the polymer to return to its permanent shape without applying an external force. Throughout the programming and recovery processes, the stationary phase can be constantly fixed to prevent molecules from irreversibly sliding during programming, so that the permanent shape can be repeatedly recovered. Taking the thermotropic SMP as an example, the stationary and reversible phases have different phase transition temperatures, denoted as T_{st} and T_{re}, respectively. Therefore, the process temperature T is between T_{st} and T_{re}, and programming and recovery can be achieved under appropriate process conditions. Because the T_g value of PET-*co*-PCL-30 % in our study was 30.3 °C, which is close to the human body temperature, this material can be used for intelligent textile applications. The shape-memory behavior of the PET-*co*-PCL-30 % dumbbell-shaped specimens and fibers was tested, and the results are presented in Figures 8-11.

The shape-memory indications are illustrated in Figure 8. The long amorphous sample obtained by quenching the just-synthesized copolymer was rolled around a glass tube (Figure 8(a)). This sample was then maintained at 120 °C ($T_{cc} < T < T_{st}$) for 2 h for recrystallization, and a permanent shape was obtained (Figure 8(b)). The sample then underwent the programming process to form its temporary shape (Figure 8(c)-(d)), which involved stretching at 100 °C ($T_{re} < T < T_{st}$) and fixing at room temperature ($T < T_{re}$) while retaining the strain by applying external force. Figure 8(d)-(f) illustrates the recovery process achieved by heating the sample in a temporary state from room temperature to 100 °C ($T_{re} < T < T_{st}$) and maintaining the temperature for 10, 20, and 30 s, respectively, without applying external force.

Figure 9 plots the R_r of PET-*co*-PCL-30 % at a 150 %

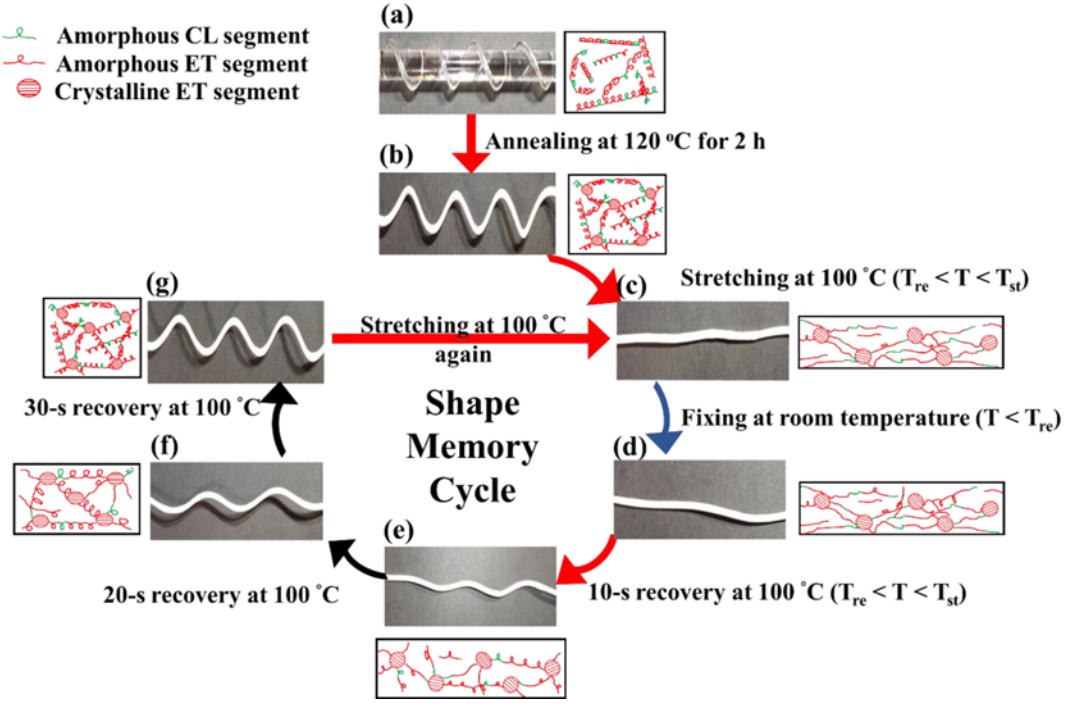

Figure 8. Shape-memory indications of a PET-*co*-PCL-30 % strand and schematic of its molecular structure in the following states; (a) quenching treatment, (b) permanent shape, (c) stretched temporary shape, (d) fixed temporary shape, (e) 10-s recovery, (e) 20-s recovery, and (f) 30-s recovery.

stretch against the recovery process time; R_r increased from 47 % to 83 % and from 51 % to 88 % for dumbbell-shaped specimens and fibers, respectively. All the samples exhibited a steady R_r value within 5 min under all the temperature conditions. This observation indicates that heating to a particular temperature provides the activation energy required to overcome the energy gap to disentangle and stretch the reversible phase; the higher the temperature applied, the more stretchable the reversible phase becomes. According to the second law of thermodynamics, the total entropy of an isolated system can never decrease. Thus, in the SMP, the disentangled and stretched temporary shaped polymer, which possesses lower entropy than the permanent shaped polymer, should recover its permanent shape naturally once the energy gap disappears. Therefore, a higher R_r value should be achieved by increasing the temperature, causing more molecules to participate in the recovery process. Notably, the temperature-dependent behavior presented here is more broad ranged different from that of conventional PCL-based thermotropic SMP, in which the crystalline phase of PCL is the reversible phase [44-46]. These phenomena ascribe the random property of the material, according to which the reversible phase is the amorphous phase of the CL segment.

The shape-memory properties of the PET-*co*-PCL-30 % copolymer under various strains and temperatures are presented in Figure 10. R_r exhibited a similar trend in all temperature ranges. When the strain level was low, a small proportion of the amorphous phase participated in the orientation. As the strain level improved to an appropriate level, the proportion of the amorphous phase participating in the orientation increased, and the degree of conformational entropy decreased; thus, the shape recovery force increased, resulting in increased R_r values. However, when strain levels were further enhanced, the weak crosslinking point between the amorphous and crystalline phases was destroyed, allowing the crystalline phase to slip, resulting in a reduction in R_r values. Therefore, 150 % is the optimal strain level for PET-*co*-PCL-30 %, which corresponds to the maximum R_r values of 82.6 % and 88.0 % for the dumbbell-shaped specimens and fibers, respectively.

The effect of the stretch-fix-recovery cycle on shape-memory performance was also investigated. The programming following the recovery process was repeated five times at a strain of 150 % and a recovery temperature of 100 °C. The R_r values of PET-*co*-PCL-30 % after different cycles are presented in Figure 11. As the number of cycles increased, the R_r value tended to stabilize. However, the few deformation

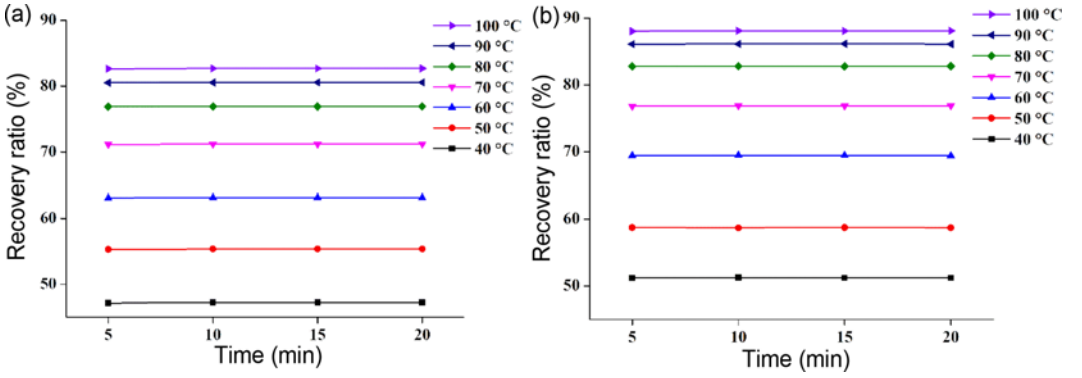

Figure 9. Effect of temperature and process time on the shape-memory performance of PET-*co*-PCL-30 % (a) dumbbell-shaped specimens and (b) fibers.

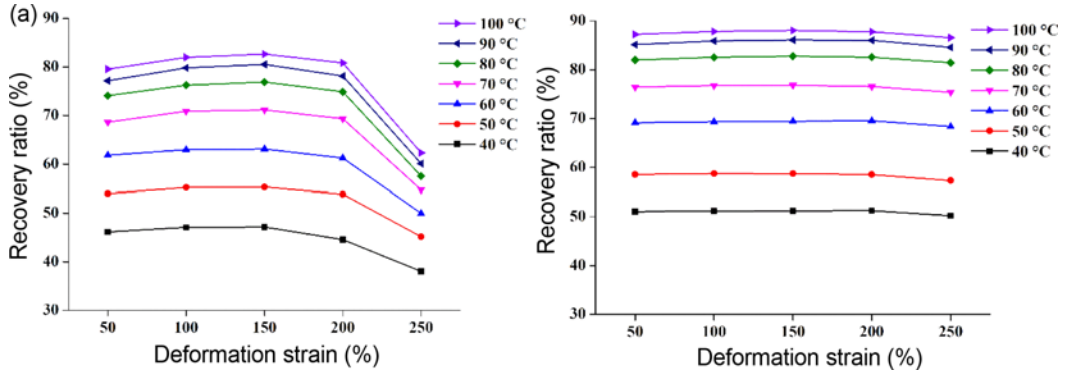

Figure 10. Effect of temperature and deformation strain on the shape-memory performance of PET-*co*-PCL-30 % (a) dumbbell-shaped specimens and (b) fibers.

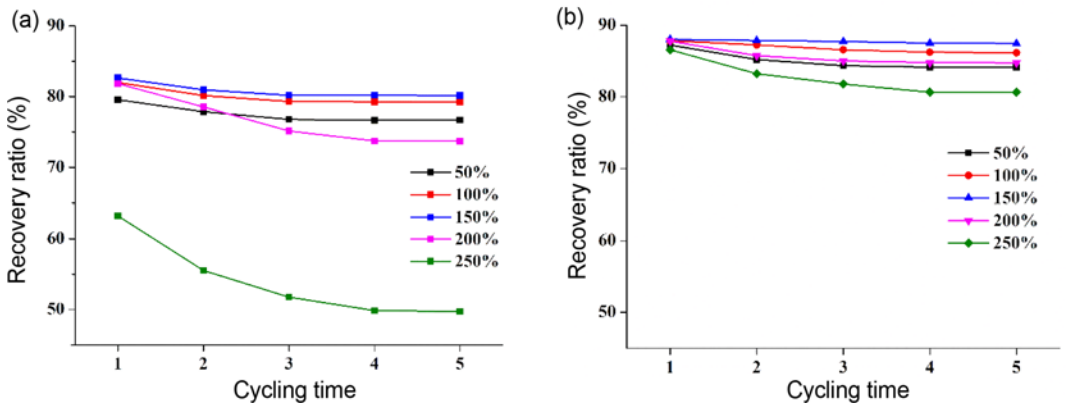

Figure 11. Effect of cycling times and deformation strain on the shape-memory performance of PET-*co*-PCL-30 % (a) dumbbell-shaped specimens and (b) fibers.

cycles destroyed the weak crosslinking points between the amorphous and crystalline phases. Moreover, because of the amorphous orientation induced by the deformation, the resistance force in the direction of deformation increased, and R_r became steady. In addition, as already mentioned in the earlier text, when the degree of deformation was greater than 200 %, because of the destruction of the crystalline phase, the shape recovery rate tended to decrease more notably during the previous cycles. However, the fiber samples were less affected by strain increments above 200 %. This behavior may have resulted from the geometry difference between dumbbell-shaped specimens and fibers. Because the circular cross section of the fibers can disperse the stress more effectively than the rectangular cross section of the dumbbell-shaped specimens, a stress concentration point is less likely to generated for the fibers, causing irreversible deformation in the crystalline phase. Therefore, when the elongation rate exceeds 200 %, the fibers exhibited no dramatic decrease in R_r compared with the dumbbell-shaped specimens.

Performance of the PET-*co*-PCL Fibers

In this study, all the PET-*co*-PCLs fibers were prepared using the melt spinning method. The process conditions are listed in Table 6. All the polymers exhibited effective processability and were spun at a winding speed of 1,000 m/min, achieving as-spun fibers of approximately 11-13 den.

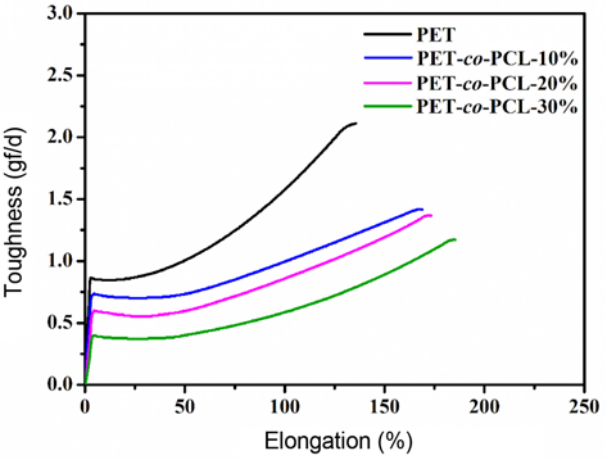

Figure 12. Stress-strain curve of PET and PET-*co*-PCL fibers.

The mechanical properties of the PET-*co*-PCLs fibers are presented in Table 7 and the stress-strain curves in Figure 12. The copolymer fibers had lower tenacity than the neat PET fiber. The addition of the CL component decreased the degree of crystallinity and intermolecular force of the fibers through the plasticizing effect.

Moreover, all the curves exhibited necking behavior, and drawing regions were observed. The stress-strain curve of these copolymers was similar to a typical PET curve. With

Table 6. Melt spinning parameters for PET and the PET-*co*-PCLs

Sample	T_m (°C)	Screw temperature (°C)	Spinneret temperature (°C)	Winding speed (m/min)	Fineness (denier)
PET	245.6	280	280	1000	13
PET-*co*-PCL-10 %	223.6	233-248	248	1000	12
PET-*co*-PCL-20 %	190.4	200-225	225	1000	12
PET-*co*-PCL-30 %	164.3	200	200	1000	11

Table 7. Mechanical properties of the PET and PET-*co*-PCL fibers

Sample	Tenacity (gf/den)	Elongation (%)
PET	2.16±0.03	133.10±0.58
PET-*co*-PCL-10 %	1.44±0.06	165.84±32.81
PET-*co*-PCL-20 %	1.42±0.11	175.19±40.32
PET-*co*-PCL-30 %	1.20±0.04	185.70±16.05

the increasing CL content, the drawing region improved, and the necking position of the PET-*co*-PCL fibers slightly reduced (Figure 12). According to Yildirim's model, this finding indicated that the introduction of short aliphatic CL chains resulted in a more irregular arrangement of molecular levels in the PET-*co*-PCL fibers; thus, more minor crystallization occurred in the PET-*co*-PCL fibers than in a homogenous PET fiber during the melt spinning process at a fixed winding speed of 1,000 m/min. Although the tenacity of the copolymer fibers seemed to be low, all the samples were as-spun without further drawing. The tenacity of the as-spun fibers was improved by heat drawing treatment at a temperature above that of the T_g of the fibers. The general requirement of 3 gf/den for a drawn filament in textile applications might be achieved after further drawing [47].

Conclusion

A one-pot polycondensation reaction was used to successfully synthesize a novel shape-memory copolyester. The chemical structure was verified based on the infrared and NMR spectra. The T_g, T_m, and X_c of these PET-*co*-PCLs decreased with the increasing PCL content. The thermal stability of the PET-*co*-PCLs did not change substantially, especially in their long-term performance. All the PET-*co*-PCL copolymers were melt spun to a filament at a winding rate of 1,000 m/min. The PET-*co*-PCL-30 % copolymer had a T_g of 30.3 °C, which is close to body temperature, and the random characteristic of this material resulted in a shape-memory behavior that was different from that of conventional PCL-based thermotropic SMP. A broad range of properties and a reversible shape recovery ratio from 38.32 % up to 82.69 % were controlled by a recovery temperature between T_g and T_m. Because of the acceptable process temperature, tunable and reversible shape-memory behavior, and biocompatibility of the PET-*co*-PCL copolymers, these materials are suitable for use in intelligent textiles.

Conflicts of Interest

The authors declare no potential conflicts of interest.

References

1. D. E. Mouzakis, N. Papke, J. S. Wu, and J. Karger-Kocsis, *J. Appl. Polym. Sci.*, **79**, 842 (2001).
2. N. Jacquel, R. Saint-Loup, J. P. Pascault, A. Rousseau, and F. Fenouillot, *Polym.*, **59**, 234 (2015).
3. W. J. Yoon, S. Y. Hwang, J. M. Koo, Y. J. Lee, S. U. Lee, and S. S. Im, *Macromolecules*, **46**, 7219 (2013).
4. J. Wang, X. Liu, Y. Zhang, F. Liu, and J. Zhu, *Polymer*, **103**, 1 (2016).
5. J. J. Benvenuta Tapia, J. A. Tenorio-López, A. Martínez-Estrada, and C. Guerrero-Sánchez, *Mater. Chem. Phys.*, **229**, 474 (2019).
6. M. Ren, Z. Zhang, S. Wu, J. Wei, and C. Xiao, *J. Polym. Res.*, **13**, 9 (2006).
7. J. Zhou, Q. Zhu, W. Pan, H. Xiang, Z. Hu, and M. Zhu, *Macromol. Rapid Commun.*, **42**, 2000498 (2021).
8. V. Sinha, M. R. Patel, and J. V. Patel, *J. Polym. Environ.*, **18**, 8 (2010).
9. J. N. Hahladakis, C. A. Velis, R. Weber, E. Iacovidou, and P. Purnell, *J. Hazard Mater*, **344**, 179 (2018).
10. S. J. Kim, H. W. Kwak, S. Kwon, H. Jang, and S. Park, *Polymers*, **12**, 2389 (2020).
11. D. I. Collias, A. M. Harris, V. Nagpal, I. W. Cottrell, and M. W. Schultheis, *Ind. Biotechnol.*, **10**, 91 (2014).
12. A. P. Mathew, K. Oksman, and M. Sain, *J. Appl. Polym. Sci.*, **97**, 2014 (2005).
13. T. A. Hottle, M. M. Bilec, and A. E. Landis, *Polym. Degrad. Stab.*, **98**, 1898 (2013).
14. T. Iwata, *Angew. Chem. Int. Ed.*, **54**, 3210 (2015).
15. A. L. Sisson, D. Ekinci, and A. Lendlein, *Polym.*, **54**, 4333 (2013).
16. Y. Makino and T. Hirata, *Postharvest Biol. Technol.*, **10**, 247 (1997).
17. T. Y. Shih, J. D. Yang, and J. H. Chen, *Procedia Eng.*, **36**, 144 (2012).
18. M. Jikei, Y. Takeyama, Y. Yamadoi, N. Shinbo, K. Matsumoto, M. Motokawa, K. Ishibashi, and F. Yamamoto, *Polym. J.*, **47**, 657 (2015).
19. N. Stanley, G. Bucataru, Y. Miao, A. Favrelle, M. Bria, F. Stoffelbach, P. Woisel, and P. Zinck, *J. Polym. Sci. Part A Polym. Chem.*, **52**, 2139 (2014).
20. F. Awaja and D. Pavel, *Eur. Polym. J.*, **41**, 1453 (2005).
21. M. Y. Abdelaal, T. R. Sobahi, M. S. I. Makki, *Int. J. Polym. Mater.*, **57**, 73 (2008).
22. K. Y. Lim, B. C. Kim, and K. J. Yoon, *J. Appl. Polym. Sci.*, **88**, 131 (2003).
23. K. Y. Lim, B. C. Kim, and K. J. Yoon, *Polym. J.*, **34**, 313 (2002).
24. D. Saaoui, S. Benali, R. Mincheva, A. Habi, P. Dubois, and J. Raquez, *J. Appl. Polym. Sci*., **137**, 48812 (2020).
25. K. Saeed and S. Park, *Iran J. Chem. Chem. Eng*., **29**, 77 (2010).
26. C. Japu, A. Martínez De Ilarduya, A. Alla, Y. Jiang, and K. Loos, *Biomacromol.*, **16**, 868 (2015).
27. U. Wit, R. J. Müller, J. Augusta, H. Widdecke, and W. D. Deckwer, *Macromol. Chem. Phys.,* **195**, 793 (1994).

28. Y. Nakayama, W. Yagumo, R. Tanaka, T. Shinon, K. Inumaru, C. Tsutsumi, N. Kawasaki, and N. Yamano, *Polym. Degrad. Stab.*, **174**, 109095 (2020).
29. H. S. Park, J. A. Seo, H. Y. Lee, H. W. Kim, I. B. Wall, M. S. Gong, and J. C. Knowles, *Acta Biomater.*, **8**, 2911 (2012).
30. P. A. Wilbon, J. L. Swartz, N. R. Meltzer, J. P. Brutman, M. A. Hillmyer, and J. E. Wissinger, *ACS Sustain Chem. Eng.*, **5**, 9185 (2017).
31. M. Soccio, L. Finelli, N. Lotti, M. Gazzano, and A. Munari, *Eur. Polym. J.*, **42**, 2949 (2006).
32. Z. Y. Yang, Y. L. Chou, H. C. Yang, C. W. Chen, and S. P. Rwei, *J. Renewable Mater.*, **9**, 867 (2021).
33. F. W. Billmeyer Jr., *J. Polym. Sci.*, **4**, 83 (1949).
34. M. Qu, H. Wang, Q. Chen, L. Wu, P. Tang, M. Fan, Y. Guo, H. Fan, and Y. Bin, *Chem. Eng. J.*, **427**, 131648 (2022).
35. K. Espinoza-García, A. Marcos-Fernández, R. Navarro, A. Ramírez-Hernández, J. E. Báez-García, and G. Rangel-Porras, *J. Polym. Res.*, **26**, 180 (2019).
36. N. Heidarzadeh, M. Rafizadeh, F. A. Taromi, L. J. del Valle, L. Franco, and J. Puiggalí, *Polym. Degrad. Stab.*, **135**, 18 (2017).
37. H. Y. Du, L. W. Liu, F. H. Zhang, J. S. Leng, and Y. J. Liu, *Compos. Part B*, **173**, 106935 (2019).
38. X. Qi, H. Xiu, Y. Wei, Y. Zhou, Y. Guo, R. Huang, H. Bai, and Q. Fu, *Compos. Sci. Technol.*, **139**, 8 (2017).
39. W. Hu, G. Z. Lum, M. Mastrangeli, and M. Sitti, *Nature*, **554**, 81 (2018).
40. H. Xie, M. He, X.-Y. Deng, L. Du, C.-J. Fan, K.-K. Yang, and Y.-Z. Wang, *ACS Appl. Mater. Interfaces*, **8**, 9431 (2016).
41. X. Qi, X. Yao, S. Deng, T. Zhou, and Q. Fu, *J. Mater. Chem. A*, **2**, 2040 (2014).
42. W. Guo, C.-H. Lu, R. Orbach, F. Wang, X.-J. Qi, A. Cecconello, D. Seliktar, and I. Willner, *Adv. Mater.*, **27**, 73 (2015).
43. A. Lendlein and S. Kelch, *Angew. Chem. Int. Ed.*, **41**, 2034 (2002).
44. Y. J. Choi, B. K. Kim, and H. M. Jeong, *Polym. (Korea)*, **22**, 131 (1998).
45. M. Naddeo, A. Sorrentino, and A. Pappalardo, *Polymers*, **13**, 627 (2021).
46. R. Tonndorf, D. Aibibu, and C. Cherif, *Polymers*, **12**, 2989 (2021).
47. S. P. Rwei and W. P. Lin, *Text. Res. J.*, **85**, 1691 (2015).